Supporting Information

Realization of Hydrogenation-Induced Superconductivity in Two-dimensional Ti_2N Mxene

Yamin Xue[1], Zebang Cheng[1], Shunwei Yao[2], Ben Wang[1], Jiajun Jiang[1], Lin Peng[1]*, Tingting Shi[3], Jing Chen[1], Xiaolin Liu[1], and Jia Lin[1]*

[1]Department of Physics, Shanghai University of Electric Power, Shanghai 200090, China

[2]School of Physics, Sun Yat-Sen University, Guangzhou, 510275 China

[3]Department of Physics, Jinan University, Guangzhou 510632, China

*Corresponding authors:

Lin Peng, Email: plpeng@shiep.edu.cn

Jia Lin, Email: jlin@shiep.edu.cn

I. HSE06 hybrid functional calculations for band structure

This section provides an expanded analysis of the electronic structure presented in our manuscript, incorporating calculations performed with the HSE06 hybrid functional. Recognized for its enhanced accuracy in predicting band gaps, the HSE06 method was applied to offer a more detailed characterization of the electronic properties near the Fermi level, a critical aspect of our study on superconductivity in hydrogenated monolayer Ti_2N.

The results derived from the HSE06 functional reveal a band structure that is consistent with our expectations, as demonstrated in Figure S1. The metallic character of the structures is maintained, and the electronic states at the Fermi level are further elucidated, which reinforces the trends observed in our PBE-based calculations. While the manuscript primarily focuses on the PBE functional due to its computational efficiency, the supplementary HSE06 analysis serves as a critical validation of our findings. It substantiates the characteristics of the electronic states and the superconducting potential of the material, thereby adding depth and rigor to our research.

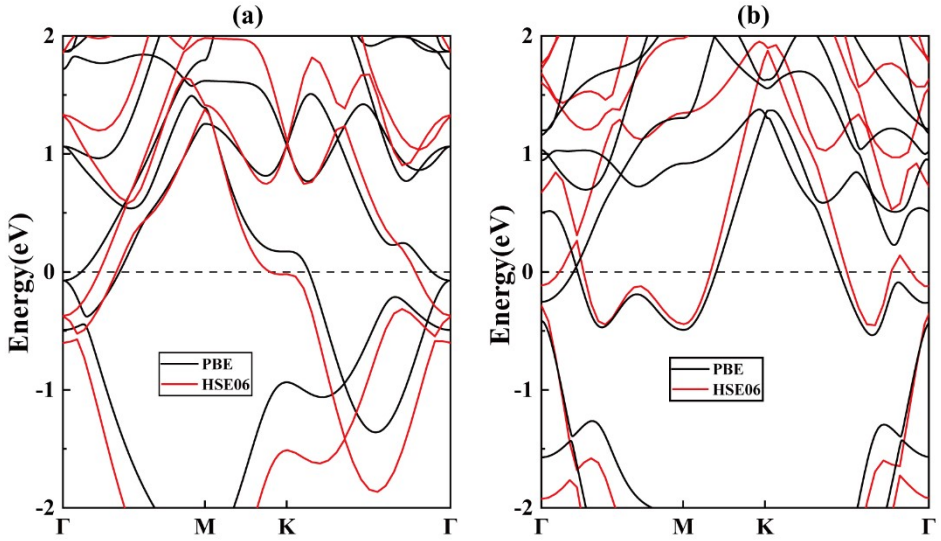

Figure S1. (a) Band structure calculated using both the PBE and HSE06 hybrid functionals for Ti_2NH_2 (b) Band structure calculated using both the PBE and HSE06 hybrid functionals for Ti_2NH_4.

II. T_c as a function of degauss for different *k*-point and *q*-point grids for Ti_2NH_4

In the investigation of the superconducting properties of Ti_2NH_4, assessing the convergence of the critical temperature (T_c) calculations is crucial. This is because T_c represents a macroscopic physical quantity dependent on the microscopic details of electron-phonon interactions, typically simulated via first-principles calculations. In these computations, the selection of *k*-point and *q*-point grids determines the sampling density of the Brillouin Zone, while the degauss parameter is used to smooth electronic state densities near the Fermi surface. Proper parameter selection is essential to ensure the accuracy of computed results, as inappropriate choices may lead to inaccuracies and impact T_c predictions. To ensure the accuracy and reliability of our computations, we conducted tests using various *k*-point and *q*-point grids (*k*:24×24×1, *q*:6×6×1; *k*:32×32×1, *q*:8×8×1; and *k*:40×40×1, *q*:10×10×1) along with a range of degauss values. As shown in Figure S2, by comparing the variations in T_c under different grid and degauss conditions, we identified a stable plateau, indicating the convergence of our calculations. Ultimately, we determined that under the *k*-point grid of 40×40×1 and *q*-point grid of 10×10×1, a degauss value of 0.04 Ry yielded a converged T_c value, providing a reliable foundation for our subsequent analyses.

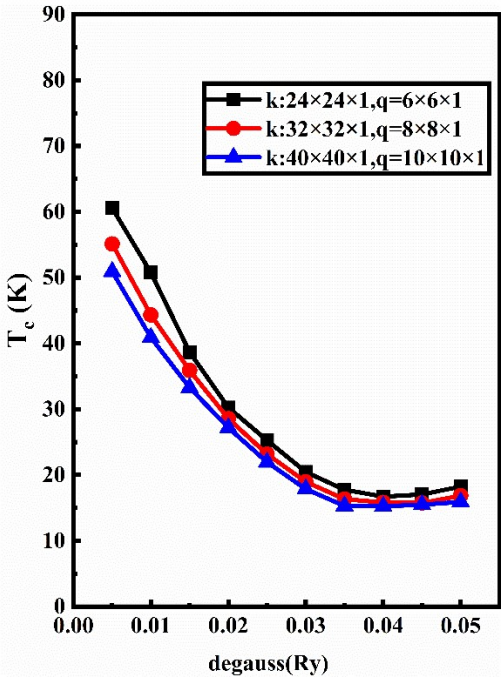

Figure S2. The variation trend of critical temperature T_c in Ti_2NH_4 under different *k*-point and *q*-point grids.

III. Influence of different μ^* values on T_c the for Ti_2NH_4 and +2% Strained Ti_2NH_4

In the Allen-Dynes modified McMillan equation, the adjustment of the Coulomb pseudopotential (μ^*) directly impacts the calculation results of T_c. μ^* quantifies the effective electron-phonon interaction generated through phonon exchange, thereby influencing the formation of Cooper pairs. Smaller values of μ^* typically enhance electron attraction, thereby favoring superconductivity, while larger values of μ^* may potentially suppress superconductivity. Figure S3 illustrates the variations of T_c corresponding to different μ^* values. In this study, we selected μ^*=0.1 for our calculations.

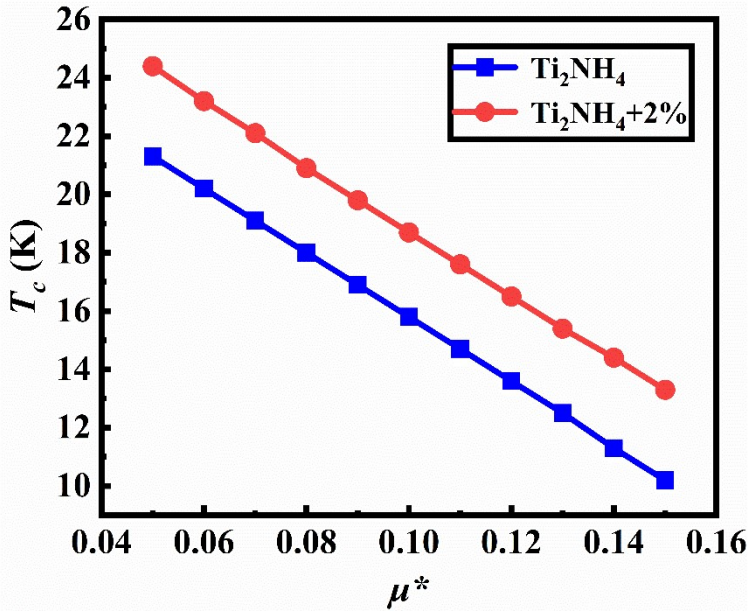

Figure S3. Variation of critical temperature T_c with different μ^* values for Ti_2NH_4 and +2% strained Ti_2NH_4.

IV. The vibration modes of pristine Ti_2NH_4 at Γ point

In Ti_2NH_4, the unit cell contains 7 atoms, which results in a total of 21 distinct phonon vibrational modes. The vibrational modes at the center of the Brillouin zone (Γ point) are detailed in Table S1. This table provides a comprehensive analysis of the vibrational modes, encompassing their frequencies, symmetries, vibration, and their infrared and Raman (IR) spectroscopic activities.

TABLE S1 The frequency (in cm^{-1}), symmetry, vibration, and activity (I and R represent infrared and Raman activity, respectively) for the 21 vibration modes at Γ point.

Modes	Freq.(cm^{-1})	Symmetry	Vibration	Activity
1	0	B_u	Translational	I
2	0	B_u	Translational	I
3	0	A_u	Translational	I
4	113	A_g	In-plane Ti and H	R
5	118	B_g	In-plane Ti and H	R
6	312	A_g	Out-of-plane Ti and H	R
7	443	A_u	In-plane N and H	I
8	445	B_u	In-plane N and H	I
9	476	A_g	In-plane H	R
10	485	B_g	In-plane H	R
11	603	B_u	Out-of-plane N and H	I
12	650	A_u	In-plane H	I
13	674	B_u	In-plane H	I
14	722	A_g	Out-of-plane H	R
15	755	B_u	Out-of-plane H	I
16	1023	A_g	Out-of-plane H	R
17	1040	B_u	Out-of-plane H	I
18	1356	A_g	In-plane H	R
19	1365	B_g	In-plane H	R
20	1369	B_u	In-plane H	I
21	1380	A_u	In-plane H	I

V. Phonon Instabilities in Ti_2NH_4 under +5% Tensile Strain

The phonon dispersion curves for Ti_2NH_4 under a tensile strain of ε = +5% are presented in Figure S4. The manifestation of an imaginary frequency within the low-frequency domain is indicative of the material's dynamical instability.

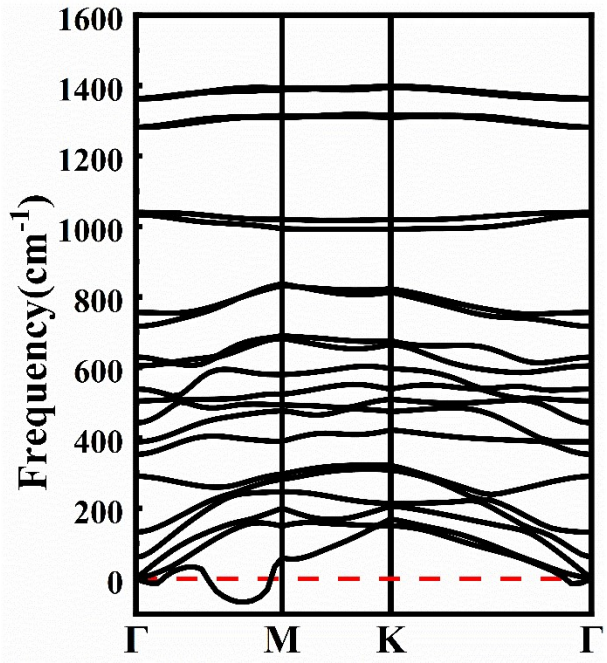

Figure S4. Phonon dispersion for compressive strain ε = +5% of Ti_2NH_4.

VI. Electron-Phonon Coupling and Superconductivity Possibility in 2% Strained Ti_2NH_4

The phonon dispersion, phonon density of states (phonon DOS), Eliashberg spectral function $\alpha^2F(\omega)$ and electron-phonon coupling (EPC) function $\lambda(\omega)$ of Ti_2NH_4 are displayed in Figure S5. The absence of imaginary frequency in the low-frequency region justifies its dynamical stability.

In the low-frequency region (0-337 cm^{-1}), the Eliashberg spectral function is predominantly driven by the coupling of electrons with the in-plane and out-of-plane vibrations of H and Ti atoms. The vibrations significantly contribute to the EPC, with a coupling strength (λ) of 0.857, representing 57.68% of the total EPC. This highlights the pivotal role of low-frequency vibrations in the genesis of superconducting properties.

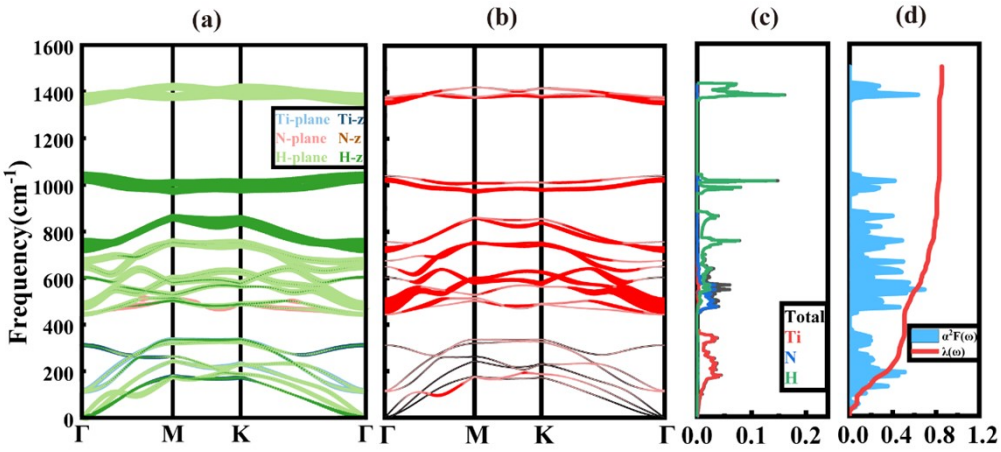

Figure S5. (a) Phonon dispersion weighted by the vibrational modes of Ti, N, and H atoms. (b) Phonon dispersion weighted by the phonon linewidth γ_{qv}. (c) Total and atom-projected phonon DOS. (d) Eliashberg spectral function $\alpha^2F(\omega)$ and cumulative frequency-dependent EPC function λ(ω) under tensile strain ε=2% of Ti_2NH_4.